Spatial correlation of precipitating and trapped protons associated with an isolated substorm

J.-M. Jahn,[1] C. J. Pollock,[1] T. J. Immel,[2] and S. B. Mende[2]

Received 3 February 2006; revised 24 April 2006; accepted 22 May 2006; published 2 August 2006.

[1] We compare the global morphology of medium energy (few keV) energetic neutral atom measurements from IMAGE/MENA with proton aurora measurements from IMAGE/FUV and in situ energetic proton data from LANL/SOPA before and during a magnetospheric substorm that commenced at 1245 UT on 19 September 2000. In the hours before substorm onset, several small auroral activations occurred at locations scattered around local midnight. The neutral atom (ENA) emissions increased continuously throughout the substorm growth phase, mimicking the pseudo-breakup behavior seen in the proton aurora and in situ energetic particle data. Half an hour before substorm onset, the rate of ENA flux increase accelerated. The substorm onset is characterized by a rapidly expanding proton aurora brightening starting near 22 magnetic local time. ENA fluxes continued to rise until 30 minutes after onset. Throughout the whole event the local time distribution of ENA and auroral emissions was remarkably similar.
Citation: Jahn, J.-M., C. J. Pollock, T. J. Immel, and S. B. Mende (2006), Spatial correlation of precipitating and trapped protons associated with an isolated substorm, *Geophys. Res. Lett.*, *33*, L15102, doi:10.1029/2006GL025917.

1. Introduction

[2] It has been demonstrated that energetic neutral atom (ENA) images can be used to observe various aspects of magnetospheric substorm activity [*Henderson et al.*, 1997; *Pollock et al.*, 2001; *C:son Brandt et al.*, 2002a, 2002b; *Pollock et al.*, 2003]. A first direct comparison between integrated proton auroral fluxes and integrated ENA fluxes during a substorm was presented by *Mende et al.* [2002] using IMAGE HENA [*Mitchell et al.*, 2000] neutral atom as well as IMAGE FUV [*Mende et al.*, 2000a, 2000b] proton aurora data. That report identified similarities of gross features prior and during a substorm, concentrating on ENAs of energies >10 keV. *Perez et al.* [2004] expanded comparisons to different phases of geomagnetic storms, using equatorial plasma distributions derived from ENA inversions. Within the uncertainties of ENA inversion techniques they demonstrated that trapped and precipitating populations occur at similar latitude and local time ranges. The correlation was better for lower (below ≈20 keV) than for higher energy ENAs.

[3] Energetic neutral atom (ENA) imaging observations are inherently difficult to interpret. The directions from which particles arrive are known well, yet the distances from the observer to the source regions, and thus the source locations, are not known a priori. They can also not be deduced trivially. To remedy this, mathematical inversion techniques have been used to recover the source population distribution of plasma from observed ENA fluxes [e.g., *Perez et al.*, 2001; *C:son Brandt et al.*, 2002a]. To reconstruct a truthful representation of the source ion distribution, high-fidelity input data with a sufficient signal-to-noise ratio are required. Especially in the case of isolated substorms, which produce much lower ENA fluxes than storm-time ring current emissions, a sufficient signal can often only be achieved by time-integration over several consecutive measurements. This degrades the capability to correlate with the rapid changes in auroral activity associated with substorms. Analyzing raw ENA data instead allows a more direct comparison between auroral and ENA imaging results, with little need for time-averaging and no need for image inversion. Even though, one has to be aware of uncertainties in ENA image data. Energy dispersion and angular scattering will occur at the entrance of current carbon-foil based instruments, finite resolution in determining particle trajectories and energies increases the imaging uncertainties, and poor counting statistics combined with undesirable background signals (charged particles; solar UV) can at times degrade imaging capabilities.

[4] To compare spatial features between both imaging techniques, we have adapted the keogram technique to ENA images. Figure 1 shows a fisheye projection of ENA emissions as seen by MENA [*Pollock et al.*, 2000], with dipole-field lines added for $L = 4$ and $L = 8$ at noon, dawn, midnight, and dusk for visual reference. Field lines in the noon meridian are plotted in red, those in the dawn meridian (positive SM y-direction) in yellow. The color scale represents the average energy flux over the measurement interval per pixel. The purple overlay indicates a grid used to rebin the ENA data. The center of the grid is located at the center of Earth's disc. For this study, we use local time keograms with 24 local time bins. The fluxes from all pixels falling within a keogram bin are summed and normalized by the number of pixels used, yielding an average energy flux for each of the local time bins. For images taken directly over the magnetic pole, such binning provides good accuracy in assigning magnetic local times. For spacecraft locations away from the pole, an increasing error in magnetic local time for a given pixel can be expected due to the line-of-sight integration nature of the data.

2. Event Overview

[5] On September 19, 2000, an isolated substorm occurred late in the recovery phase of a magnetic storm. *Dst* had

[1]Space Science Department, Southwest Research Institute, San Antonio, Texas, USA.
[2]Space Sciences Laboratory, University of California, Berkeley, California, USA.

0094-8276/06/2006GL025917$05.00

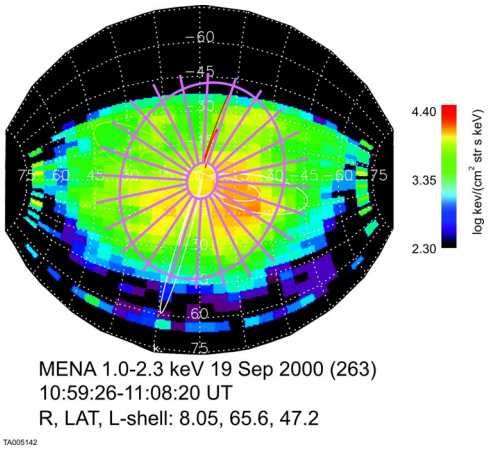

Figure 1. Schematic on how keograms are calculated based on global observations of ENA emissions.

reached a minimum of −201 nT during the last hour of September 17, 2000, but had recovered to −68 nT at the time of substorm onset. The substorm onset itself occurred at 1242 UT, derived from both in situ energetic proton injections observed at geosynchronous altitudes by Los Alamos (LANL) energetic particle detectors and from global auroral imaging by the FUV instrument onboard the IMAGE spacecraft. Solar wind data from ACE at the L1 point (Figure 2e) indicate that, after a last excursion to near-zero values at 1003 UT, southward interplanetary magnetic field (IMF) conditions prevailed until 1424 UT (except for two momentary excursions to $B_z \approx 0$ nT at 1142 and 1236 UT). All ACE measurements are time shifted to account for transport to the magnetopause. During the hour before substorm onset, B_z^{GSM} slowly changed from −7 nT to −4 nT. These IMF conditions caused prolonged driving of the magnetosphere prior to and throughout the substorm event. At 1236 UT, six minutes before substorm onset, a brief excursion of B_z to near-zero values could, within the errors of propagating the solar wind data, be regarded as a possible trigger of the substorm. IMF B_y was negative from 0729 UT until 1139 UT, when it started a quasi-periodic oscillation between positive and negative B_y values with a period of 25–30 minutes. All minima of this oscillation were located around $B_y \approx -3.5$ nT, while the maxima cover a range of +0.5 to +3.0 nT. The solar wind was moderately fast around this substorm event, with $v_{SW} = 650$ km s^{-1} at onset and a slow decay rate of 10 km · s^{-1} per hour throughout the event. The solar wind density was 6–8 cm^{-3}.

[6] During continuous negative B_z^{GSM} conditions leading to substorm onset at 1242 UT, a series of substorm-like activations can be seen both in situ and remotely. Los Alamos geosynchronous observations show the enhancement of energetic protons at 0947, 1024, and approximately 1130 UT (Figures 2c and 2d). Likewise, FUV proton aurora observations show corresponding pseudo-breakup type signatures at 0950, 1027, and 1130 UT. All LANL instruments also detected a fourth activation centered near 1202 UT, which may coincide with a weak proton aurora enhancement between local midnight and 03 magnetic local time (MLT) at approximately the same time.

[7] Figures 2a and 2b show the ENA (1.0–2.3 keV) and FUV mean fluxes per pixel for the 20–24 (red) and 24–04 (blue) magnetic local time sector. Vertical dotted lines indicate the four activations identified above, the vertical line at 1242 UT marks the substorm onset, and the dashed line at 0906 UT calls out the time when ENA fluxes start to increase significantly for the first time. As described above, pre-substorm auroral activity was more pronounced in the post-midnight sector.

[8] The ENA fluxes reflect some of this activity, though their response to individual auroral activations is comparatively weak. The main feature in the ENA data is a 4-hour long, continuous flux increase that suddenly started at ~0906 UT. The onset of this increase coincides with the arrival of a distinct jump in the IMF (B_z from +5.0 to −2.0 nT, B_y from −5.0 to −9.0 nT).

3. Discussion

[9] It has been previously shown [*Mende et al.*, 2002] that there is a correlation between proton aurora fluxes and

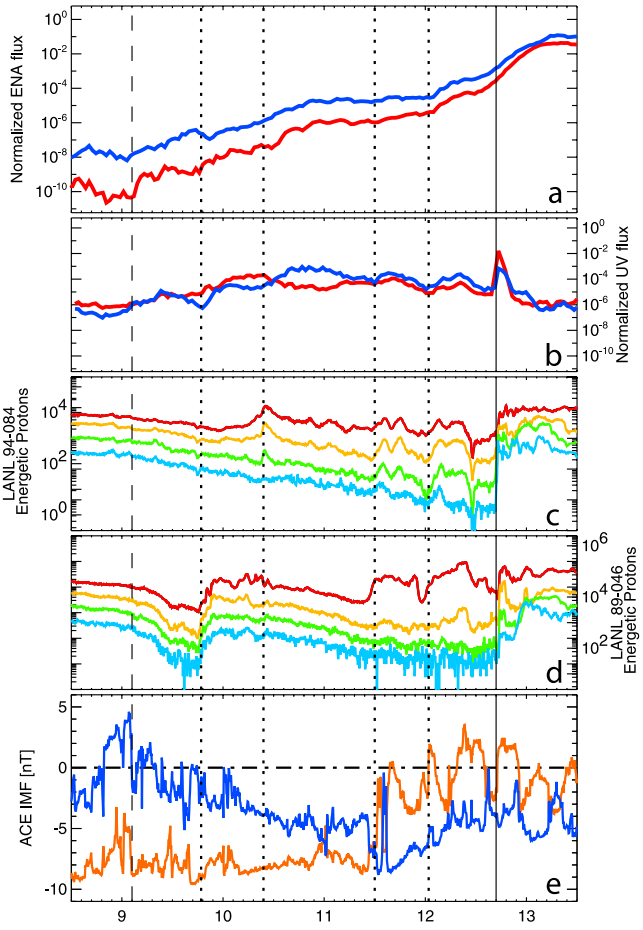

Figure 2. Solar wind and magnetospheric measurements around the September 19 substorm. (a) Normalized 1.0–2.3 keV ENA flux for 20–24 LMT (red) and 24–04 MLT (blue); (b) normalized proton aurora UV flux for 50–70° latitude for same local time ranges as for ENAs; (c and d) Los Alamos geosynchronous SOPA energetic proton measurements for satellites 94-084 and 89-046; (e) solar wind IMF B_z (blue) and B_y (orange) from ACE, shifted to the magnetopause. The approximate MLT for Los Alamos data is UT+7.0 hours for 94-084, and UT-11.0 hours for 89-046, respectively.

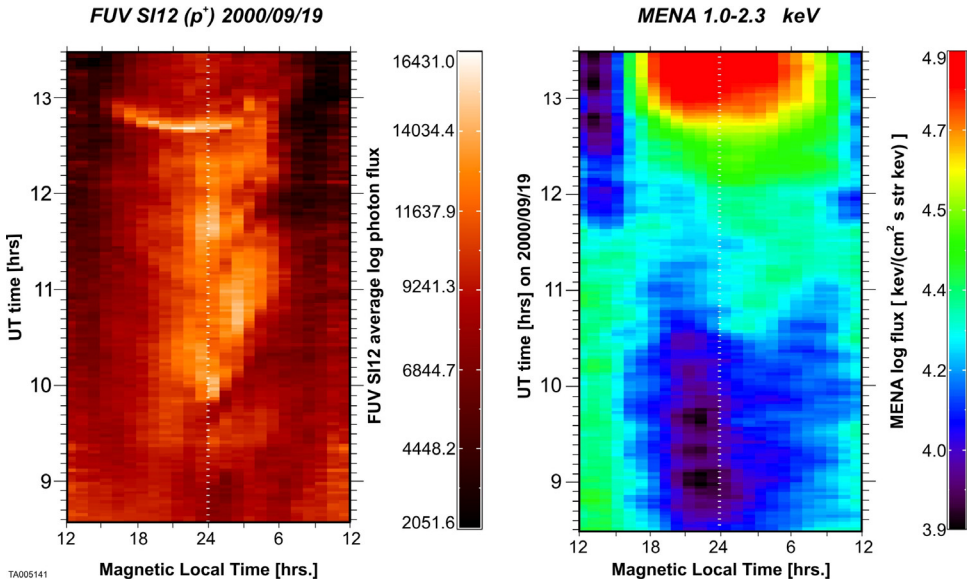

Figure 3. (left) Keograms of integrated proton aurora fluxes and (right) medium energy ENA fluxes as a function of magnetic local time and UT time. Onset of the substorm proper is at 1242 UT, toward the top of both spectrograms.

higher energy (10's of keV and up) ENA fluxes during this substorm. We expand these observations both in energy and scope, looking for spatial correlations between "trapped" (in the sense of non-precipitating) particle populations represented by ENA measurements at plasma sheet energies, and precipitating ion populations detected by proton auroral imaging.

[10] The substorm event presented here exhibits some characteristics less commonly observed in an average isolated substorm: (a) Onset is preceded by an extended growth phase (several hours of southward IMF) interdispersed with pseudo-breakup auroral activity, (b) the expansion phase auroral brightening encompasses nearly 12 hours of magnetic local time, and (c) energetic particles respond to the onset at all observed local times, including dayside.

3.1. Growth Phase

[11] The extended substorm growth phase is caused by a prolonged southward IMF interval preceding the event. The effect of southward IMF can be seen in the energetic proton data from all available LANL detectors. As B_z turns southward at 0906 UT, a characteristic drop-out in energetic particle flux develops (see for example detector 89–046 which, at 0906 UT, was located near 22 MLT). These dropouts have been associated with the stretching of the nightside magnetic field lines [*Sergeev et al.*, 1992]. Note that the IMF B_z had not yet permanently settled on a southward direction until about an hour later.

[12] Southward IMF conditions cause enhanced convection in the magnetosphere. Sustained increases in convection will result in more plasma sheet material penetrating deeper into the inner magnetosphere. This plasma will encounter increased geocoronal densities, giving rise to increased rates of charge exchange. We therefore should expect to see an increase of ENA fluxes. Figure 2 shows that in the 3.5 hours between 0906 UT and substorm onset at 1242 UT we observe an increase in ENA fluxes on the nightside by at least one order of magnitude. The flux increase is steady, though slower between ~1120–1200 UT. More ENA flux is observed at post-midnight, however the ratio of post- to pre-midnight fluxes is decreasing as the event progresses. It should be noted that during the study interval IMAGE is located near apogee of its highly elliptical orbit. The orbital motion of the spacecraft does not explain the observed flux changes through simple viewing geometry effects (examining control days with similar orbits supports this statement). Likewise, if the magnetosphere is observed from similar orbital positions in the absence of enhanced convection (and an otherwise magnetically quiet magnetosphere) ENA emissions will be both significantly lower and not increasing over time.

[13] To examine spatial correlation between auroral and ENA observations, we use keogram displays of the data. Figure 3 (left) shows the magnetic local time—UT keogram of the FUV SI12 proton aurora data. The logarithmic color scale corresponds to the total proton auroral imager's response integrated over 50° to 70° latitude, binned into one-hour local time bins. The dotted line in the center indicates local midnight. Near the top of the panel, at 1242 UT, the substorm onset can be identified by an auroral brightening occurring at 23 MLT, quickly expanding toward dawn and dusk and eventually reaching across the nightside from approximately 16 MLT to 03 MLT (possibly extending to 05 MLT) after only 10 minutes.

[14] The observed pre-onset activations appear as localized UV flux enhancements in the proton aurora keogram. The first activation at 0950 UT occurs at local midnight and expands mostly toward dusk, while the second activation at 1027 UT starts at 03 MLT and expands mostly toward dawn. Both activations are visible for about 45–50 minutes. The third activation at approximately 1130 UT is less structured. It is centered around local midnight, with a small excursion toward dawn. A fourth activation is visible starting at about 1206 UT, yet it is considerably weaker and more shortlived than the previous three activity periods.

[15] Figure 3 (right) shows the corresponding MENA ENA flux keogram for 1.0–2.3 keV neutral atoms. Vertical and horizontal ranges are identical to the ranges of the auroral keogram. The color scale indicates average ENA flux per $4^\circ \times 5^\circ$ pixel binned into one hour magnetic local time bins as described in the previous section. The keogram does not capture well the low-level ENA activity before ~1030 UT that we described for Figure 2, but it confirms that prior to onset more ENA emissions are observed post- rather than pre-midnight. (Emissions which are visible until 1150 UT at the far edges of the keogram near local noon are caused by sunlight contamination in the original ENA images.) For the auroral activations at 1027 and 1130 UT the location and spatial development of auroral dynamics is also observed in the ENA data. This suggests that ENA measurements detect plasma on roughly the same field lines that connect to the regions of proton precipitation.

3.2. Onset, Expansion, and Recovery

[16] With substorm onset, similarities and differences between auroral precipitation and ENA observations become more pronounced. Substorm onset in the proton aurora data is not only rapid, but the subsequent expansion of the auroral brightening reaches unusually far, encompassing almost 12 hours of local time. The aurora disappears as quickly as it appeared, 18 minutes after onset the emission level has dropped back to pre-event levels from four hours earlier.

[17] In some ways, the ENA signature is very different from the auroral signature. The auroral onset is, in terms if ENA flux, very indistinct (see Figure 2). While the auroral emissions are intense but short-lived, the ENA flux increase is significant but slow. It starts gradually about 10 minutes prior to substorm onset, remains strong through the time of auroral brightening, and continues after auroral emissions have all but disappeared. ENA fluxes reach their maximum about 36 minutes after onset, then slowly start to decrease. This recovery phase decrease would typically take 1–2 hours. However, shortly after 1330 UT MENA entered a region of intense high-energy plasma, swamping the detector with energetic ions and preventing further imaging of the magnetosphere. We compared this substorm to smaller isolated substorms on other days and found that all events show similar emission profiles both for the rise and the decay of ENA emissions. This is not really surprising, as "low energy" plasma sheet particles have been shown not to participate in dispersionless energetic particle injections (above 10's of keV) typical of substorms [*Birn et al.*, 1997]. Instead, the increase of ENA fluxes can be viewed as evidence of plasma sheet material moving closer to Earth, into a region of higher geocoronal density. HENA observations reported by *Mende et al.* [2002] predominantly showed ENA observations from higher energy particle populations which do participate in dispersionless substorm injections and subsequent gradient-curvature drift around Earth.

[18] While the timing of auroral and ENA signatures is quite different, the spatial distribution of emissions during the substorm is not. The local time range of maximum extension of the auroral brightening and of the ENA emissions is almost identical. This could mean that the precipitation occurs near the leading edge of the plasma sheet detected by ENA emissions. If no refilling of the loss cone occurs, precipitation will quickly subside while the remaining trapped (i.e., mirroring) particle populations will continue to produce ENAs through charge exchange.

4. Summary

[19] We present an isolated substorm during a time of extended southward IMF, causing enhanced convection in the magnetosphere. The substorm is preceded by several auroral pseudo-breakups that are also evident in both in situ energetic particle data from geosynchronous orbit and in the energetic neutral atom imaging observations. The ENA observations presented here focus on the dynamics of the plasma sheet rather than that of energetic (mostly gradient-curvature drifting) plasmas. We detect both clear similarities and significant differences between ENA and auroral observations. In the growth phase leading to substorm onset, several pseudo-breakups can be observed in both the auroral imaging and the ENA data. While the ENA fluxes are weak, they occur at the same local times as the auroral precipitation. The entire growth phase is marked by a continuous increase in ENA fluxes. Onset itself causes a rapid and unusually wide (in MLT) brightening of the aurora that quickly fades after reaching its peak. ENA fluxes do not show the onset itself, rather a steepening increase of flux lasting for over half an hour past the substorm onset. The subsequent decay of emissions is slow. Throughout the substorm growth, expansion and recovery phase, the local time ranges of auroral and ENA emissions almost always overlap remarkably well.

[20] **Acknowledgments.** We would like to thank the ACE mission for providing solar wind measurements, and Heather Elliott for her help in preparing ACE solar wind data. We also would like to thank Mike Henderson for providing Los Alamos geosynchronous SOPA data. This research was supported by the NASA IMAGE mission under NAS5-96020.

References

Birn, J., M. F. Thomsen, J. E. Borovsky, G. D. Reeves, D. J. McComas, and R. D. Belian (1997), Characteristic plasma properties during dispersionless substorm injections at geosynchronous orbit, *J. Geophys. Res.*, *102*(A2), 2309–2324.

C:son Brandt, P., R. Demajistre, E. C. Roelof, S. Ohtani, D. G. Mitchell, and S. Mende (2002a), IMAGE/high-energy energetic neutral atom: Global energetic neutral atom imaging of the plasma sheet and ring current during substorms, *J. Geophys. Res.*, *107*(A12), 1454, doi:10.1029/2002JA009307.

C:son Brandt, P., S. Ohtani, D. G. Mitchell, R. Demajistre, and E. C. Roelof (2002b), ENA observations of a global substorm growthphase dropout in the nightside magnetosphere, *Geophys. Res. Lett.*, *29*(20), 1962, doi:10.1029/2002GL015057.

Henderson, M. G., G. D. Reeves, H. E. Spence, R. B. Sheldon, A. M. Jorgensen, J. B. Blake, and J. F. Fennell (1997), First energetic neutral atom images from Polar, *Geophys. Res. Lett.*, *24*(10), 1167–1170.

Mende, S. B., et al. (2000a), Far ultraviolet imaging from the IMAGE spacecraft. 1. System design, *Space Sci. Rev.*, *91*(1–2), 243–270.

Mende, S. B., et al. (2000b), Far ultraviolet imaging from the IMAGE spacecraft. 3. Spectral imaging of Lyman-α and OI 135.6 nm, *Space Sci. Rev.*, *91*(1–2), 287–318.

Mende, S. B., H. U. Frey, T. J. Immel, D. G. Mitchell, P. C:son Brandt, and J.-C. Gèrard (2002), Global comparison of magnetospheric ion fluxes and auroral precipitation during a substorm, *Geophys. Res. Lett.*, *29*(12), 1609, doi:10.1029/2001GL014143.

Mitchell, D. G., et al. (2000), High energy neutral atom (HENA) imager for the IMAGE mission, *Space Sci. Rev.*, *91*(1–2), 67–112.

Perez, J. D., G. Kozlowski, P. C:son-Brandt, D. G. Mitchell, J.-M. Jahn, C. J. Pollock, and X. X. Zhang (2001), Initial ion equatorial pitch angle distributions from medium and high energy neutral atom images obtained by IMAGE, *Geophys. Res. Lett.*, *28*(6), 1155–1158.

Perez, J. D., X.-X. Zhang, P. C:son Brandt, D. G. Mitchell, J.-M. Jahn, C. J. Pollock, and S. B. Mende (2004), Trapped and precipitating protons in the inner magnetosphere as seen by IMAGE, *J. Geophys. Res.*, *109*, A09202, doi:10.1029/2004JA010421.

Pollock, C. J., et al. (2000), Medium energy neutral atom (MENA) imager for the IMAGE Mission, *Space Sci. Rev.*, *91*(1–2), 113–154.

Pollock, C. J., et al. (2001), First medium energy neutral atom (MENA) images of Earth's magnetosphere during substorm and storm-time, *Geophys. Res. Lett.*, *28*(6), 1147–1150.

Pollock, C. J., et al. (2003), The role and contributions of Energetic Neutral Atom (ENA) imaging in magnetospheric substorm research, *Space Sci. Rev.*, *109*(1), 155–182.

Sergeev, V. A., T. Bösinger, R. D. Belian, G. D. Reeves, and T. E. Cayton (1992), Drifting holes in the energetic electron flux at geosynchronous orbit following substorm onset, *J. Geophys. Res.*, *97*(A5), 6541–6548.

T. J. Immel and S. B. Mende, Space Sciences Laboratory, University of California, Berkeley, 7 Gauss Way, Berkeley, CA 94720–7450, USA.

J.-M. Jahn and C. J. Pollock, Space Science Department, Southwest Research Institute, 6220 Culebra Rd., San Antonio, TX 78253, USA. (jjahn@swri.edu)